Application of d.c. Plasma Arc Heating to Hypersonic Propulsion Testing

S. D. RAEZER,* E. A. BUNT,† AND H. L. OLSEN‡
The Johns Hopkins University, Silver Spring, Md.

As propulsion testing is undertaken at lower altitudes and higher Mach numbers, the requirements of correct static temperature and pressure simulation and uniform flow in a test section of practical size lead to stagnation temperatures too high to be produced by storage-type heaters. For this reason, a 10-Mw d.c. plasma arc heater has been developed for use with a Mach 7 to 10 tunnel. Thermal efficiencies exceeding 60% have been achieved at useful flight simulation conditions. The design principles and operating characteristics of the integrated arc heater and hypersonic propulsion tunnel are described in some detail.

Nomenclature

A = exit nozzle area, in.^{2}
E = potential, v
h = enthalpy, Btu-lb^{-1}
i = current, amp
l = length, in.
$\dot{m}$ = weight flow, lb-sec^{-1}
M = Mach number
n = number of cells
P = pressure, psia
Pr = Prandtl number
r = total circuit resistance, Ω
Re = Reynolds number
T = temperature, °R
V = velocity, ft-sec^{-1}
γ = ratio of specific heats
δ = boundary-layer thickness, ft
δ^* = boundary-layer displacement thickness, ft
ϵ = efficiency, power out/power in
μ = dynamic viscosity, lb-ft^{-1}-sec^{-1}
ρ = weight density, lb-ft^{-3}

Superscript

* = throat condition, where $M = 1$, except for δ^* above

Subscripts

b = battery no-load condition

Introduction

THE Applied Physics Laboratory of the Johns Hopkins University has long been active in ramjet propulsion research and development, which involves the ground testing of models and components under simulated flight conditions. About three years ago, steps were taken to provide test capabilities for the hypersonic flight speed regime from Mach 5 to 10 or higher. The main objective was to simulate atmospheric static pressure and temperatures for inlet and combustion testing of air-breathing engines and components for periods of the order of 1 min. Unfortunately, the stagnation temperatures characteristic of hypersonic flight at Mach numbers above 7 or 8 are beyond the capabilities of pebble bed, electrical resistance, or "chemical" heaters. For example, at Mach 10 and an altitude of 155,000 ft, the required stagnation pressure and temperature are 2500 psia and 7500°R, respectively, and for a propulsion tunnel of sufficient size to yield practical test results operating at simulated altitudes around 100,000 ft, the heater must yield an exit heat flow of about 6000 Btu/sec (~6 Mw). Surveys of possible tunnel-heater combinations showed that the plasma arc was the only heat source likely to be able to provide the simulation conditions required by this phase of the research program. Consequently, the task of developing a suitable high-pressure, high-power arc heater was undertaken, because no such device was in existence at that time. Preliminary work on small-scale arc heaters[1] was undertaken in a prototype facility at the Forest Grove Station concurrent with the early stages of the design of a new Propulsion Research Laboratory. The work reported herein has been performed largely at the new laboratory.

The main requirement (which has now been met) has been that of simulating certain conditions specified in area A in the altitude-Mach number diagram§ (Fig. 1), namely, those relating to operation at Mach numbers of 7 and 10. This figure gives the stagnation temperature, pressure, and weight flow for a 1-ft^2 test section (inviscid flow equivalent). The boundaries of area A were determined partly by previously planned ejector capability (vacuum level, upper limit; and weight flow, left-hand limit) and partly by extrapolation of the state-of-plasma arc technology at the time. The lower limit (output power into gas) was chosen as 6 Mw, since carbon-electrode arc heaters had already been operated at input powers up to 15 Mw. The required enthalpy was relatively low, the value for Mach 10 operation being about 2500 Btu-lb^{-1}. To date the program has resulted in the achievement of arc operation at pressures, enthalpies, air mass flows, and running times sufficient to meet the original objective. Arc operation at pressures in area B is currently being investigated experimentally, and facility provision for higher pressure operation (area C, 2500–5000 psia) at present is also being made. Although the arc development work is continuing, it is thought to have reached a stage of sufficient interest to warrant the present report.

Presented as Preprint 63122 at the AIAA-ASME Hypersonic Ramjet Conference, White Oak, Md., April 23–25, 1963; revision received January 2, 1964. This work was supported by the Bureau of Naval Weapons, Department of the Navy, under Contract NOw 62-0604-c. The authors would like to express appreciation to W. H. Avery, Supervisor of the Aeronautics Division, and to L. O. Kauffman, C. L. Yates, M. E. Rose, W. J. Fleagle, R. G. Heidelbach, L. W. Bennett, G. A. Smoot, and R. T. Cusick for their services to the project, and particularly for assistance in the design, computation, and operation phases.

* Physicist, Propulsion Facility Group, Applied Physics Laboratory.

† Section Supervisor, Propulsion Facility Group, Applied Physics Laboratory.

‡ Group Supervisor, Propulsion Facility Group, Applied Physics Laboratory.

§ This diagram was constructed with the aid of data derived from Refs. 2 and 3.

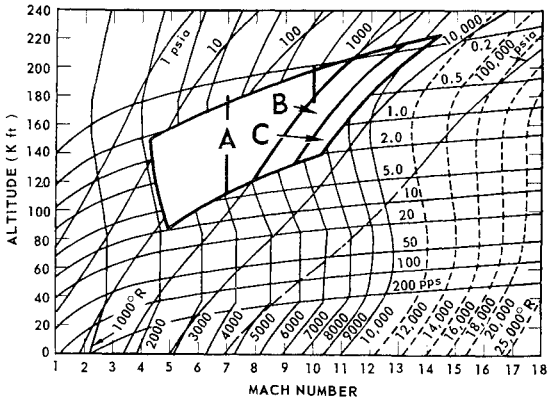

Fig. 1 Arc heater operating areas in relation to altitude and Mach number for a 1-ft² flow cross section; stagnation conditions are derived from Refs. 2 and 3.

Design and Operation

High-power arc units normally require a means of inducing arc movement to avoid rapid erosion of the electrodes. The hydrodynamic swirl (tangential gas inflow) approach, which was used in early plasma arcs for this purpose, is ineffective at pressures above a few atmospheres, and therefore magnetic rotation is employed; the driving magnetic field can be either self-induced or supplied by external coils. The electrode form chosen for the arc heater described herein (Fig. 2) is a special re-entrant arrangement of "rail accelerator" which eliminates the need for bulky field coils by making use of the magnetic field induced by the currents flowing in the electrodes. This device was originally suggested by Reid[4] of the General Electric Company, Cincinnati, for use in the latter's three-phase a.c. arc, but its operation has been improved in the APL application by running it under d.c. conditions. The splits in the electrodes necessitated by this arrangement are jumped at each revolution by the continuously rotating arc and are set 180° apart to make it easier to maintain a uniform spacing between the electrodes. Adequate arc rotational velocities result from the use of currents in excess of about 8000 amp, depending on the pressure. The roughly square electrode configuration employed has a distinct advantage over the circular in that the arc is observed to have less tendency to bow out.

The electrodes are constructed of 1-in.-o.d. copper tubes with 0.25-in. walls (selected on the basis of an analysis of the heat transfer). Water is circulated through them at a linear

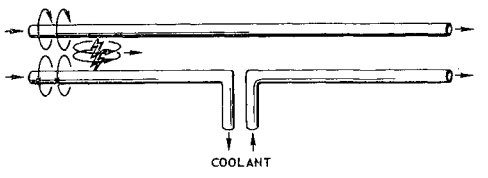

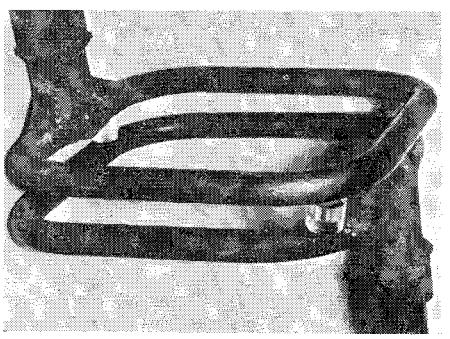

Fig. 2. Arrangement of split-ring electrodes.

velocity of the order of 120 ft-sec^{-1}. The pressure drop through the electrodes required to achieve this velocity is sustained by forcing the coolant from storage tanks by air at 1500 psia. Average heat fluxes of up to 30 Btu-in.$^{-2}$-sec^{-1} into the electrode cooling water have been observed at high-power input. During operation the electrodes are subjected to an oscillating bending moment [resulting from magnetic repulsion effects coupled with the arc rotation (Fig. 3) whose effect becomes negligible at gap lengths greater than 1.25 in. for this electrode design.

The arc chamber is a water-cooled pressure vessel which provides for heat release into the test air in a region of low-speed flow between two sonic orifices (or venturis); the upstream one is used to set the air mass flow independently of conditions in the chamber, whereas the second determines the arc chamber pressure for a given gas temperature and may also serve as the throat of the propulsion tunnel nozzle. Since flow simulation requirements may call for enthalpies below that at which it is possible to run the arc/power-supply combination, a parallel air line bypassing the arc chamber (but also containing a suitably sized sonic orifice) is available; this secondary line injects into a short mixing chamber between arc chamber and nozzle throat. The over-all design is shown in elevation in Fig. 4a. The main design features to be noted are as follows:

Electrode supports: The electrodes are cantilever-supported from the end plates. In order to minimize the tendency of the arc to "walk" along the supporting posts, these are at right angles to the electrode rings. The deepest of the three insulator sections (A, Fig. 4a) is of Micarta and forms the structural support. This is covered by a sealing section B of Lucite (chosen because it does not form a conducting char if exposed to severe heating), which in turn is protected from direct contact with chamber gases by a relatively loosely fitting cover C, for which fused silica has been found most satisfactory.

Wall cooling: Water-cooling of the chamber wall was at first done with a double-wall system using internal copper liners, but the latter were difficult to fabricate and were subject to diametral shrinkage under the cyclic operation which led to water leaks at "O" ring seals. The walls and end plates are now fabricated with internal (drilled) cooling water passageways to eliminate the possibility of water leaks into the chamber.

Insulation: In addition to the electrode insulation already noted, the arc chamber is electrically isolated from the tunnel nozzle and the air and water manifolds in order to keep the former electrically floating.

Air admission: Since the aerodynamic drag of the rotating arc sets up a gas vortex in the chamber, the flow direction of incoming air is relatively unimportant. In the present design, the air is admitted from plenum annuli formed by both end plates and their junction with the body.

Access and vent valve: A port is built into the chamber (Fig. 4a) to allow for inspection of chamber and tunnel throat and for insertion of the short-circuiting starting wire. Into this port may also be inserted the unit designated "cooled plug valve," a bleed valve which is open at the start of the run to allow the arc to become fully established while at low pressure, irrespective of mass flow.

Figure 5, a recording of pressure and voltage taken during an arc run, illustrates typical aspects of arc operation. At the moment of firing, a pressure pulse is generated in the arc chamber which may lead to an excessive voltage demand and arc blowout. This is prevented by use of the vent valve just described. After the vent valve was closed the flow was progressively increased by raising the upstream (regulated) pressure, leading to ultimate blowout for the particular combination of flow and power supply settings employed. After blowout the voltage reverts to the no-load value.

Systematic measurements of the rate of erosion of the split-ring electrodes have been difficult to obtain. Direct

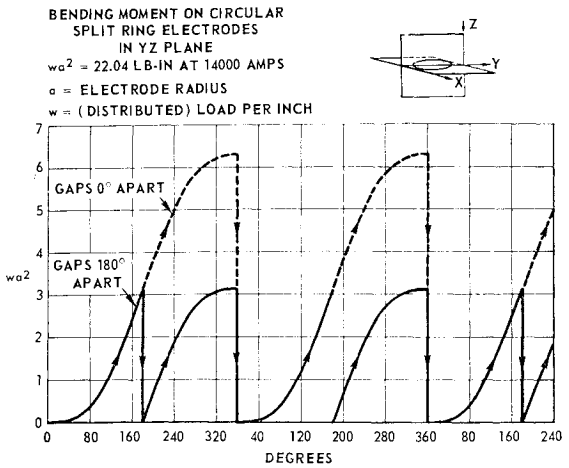

Fig. 3 Bending moment on electrodes due to magnetic repulsion.

sampling of the jet during actual running in nitrogen has shown the proportion of copper to be 30–40 parts per million, but observation of the electrodes—where the erosion is heaviest at the split—suggests that the loss of copper from the electrodes is much higher. Although no directly comparable figures are yet available for the present electrode configuration, erosion figures of about 0.05% of the air flow are estimated from the weight loss. Two possibilities may account for this discrepancy. First, much of the eroded material is trapped in the arc chamber by the action of the gas vortex, and second, erosion may be concentrated largely in the starting phase.

Efficiencies have been determined by both cooling-water calorimetry and by mass balance across two choked orifices, accounting for real gas effects. With regard to the former technique, water-temperature rises in the various components are measured by thermocouples and the power input is measured electrically.

Arc operating characteristics: The operation of a confined gas-cooled arc can be considered as known in principle if, in addition to the gas properties, the mass flux equation, the electrical circuit equation, the arc characteristic, and the heat transfer are known. A knowledge of the latter two must rely strongly on empirical information.

It was assumed that the arc characteristic could be expressed as a product function of the form

$$E = f(\dot{m})P^a i^b \tag{1}$$

An empirical fit to the data from 80 arc runs then yielded the values

$$f(\dot{m}) = (5.17 + 1.37\dot{m}) \times 10^4$$
$$a = 0.27$$
$$b = -0.70$$

in the region $0.05 < \dot{m} < 3.5$ lb-sec^{-1}, $15 < P < 1250$ psia, and $8000 < i < 20{,}000$ amp.

Using an equation of the form of (1), the St. Venant-Wantzel equation for choked flow through a nozzle,[5] the d.c. circuit equation, and the approximation $T = 150h^{1/2}$ in the region $3000 < T < 10{,}000$°R and $10 < P < 100$ atm as deduced from Hilsenrath's and Beckett's tables,[6] simple and useful solutions may be obtained for the variables of state (P, h, E, and i) in terms of the controllable parameters (E_b, r, $\dot{m}$, and A). By means of these solutions, the range of operation of the arc heater can be delineated with fair accuracy. For example, for the arc voltage, one obtains

$$\theta = \phi \tag{2}$$

where

$$\theta = (E/E_b)^x(1 - E/E_b)^{1-x}$$

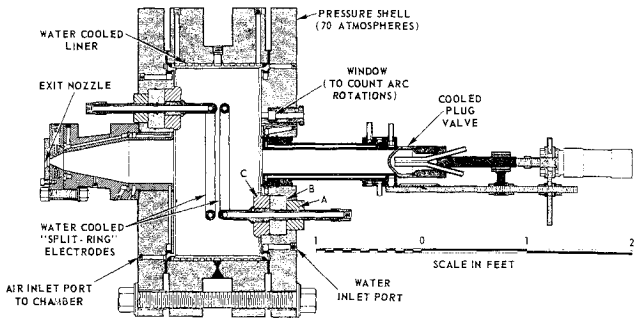

a)

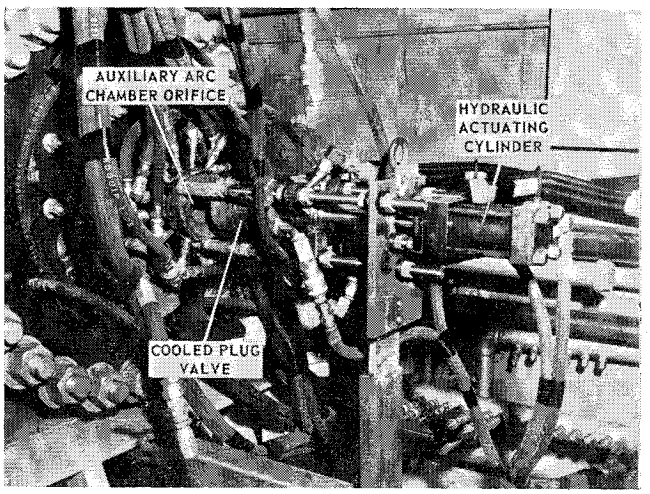

b)

Fig. 4 a) Arc chamber design; b) vent valve for starting.

and

$$\phi = (1/E_b)\{4.0A^{-1}[f(\dot{m})]^{1/a}\dot{m}^{3/4}r^{-(b/a)-1/4}\epsilon^{1/4}\}^y$$

using a γ of 1.4. Here $x = (1 - a/4)/(1 - b - a/2)$ and $y = a/(1 - b - a/2)$. By taking limits, one obtains for the maximum value of E/E_b,

$$(E/E_b)_{\max} = x \tag{3}$$

along with the additional stability criterion,

$$\phi < \theta_{\max} \tag{4}$$

In Table 1, experimentally observed values of $(E/E_b)_{\max}$ taken from blowoff runs are tabulated (along with the corresponding values of $\dot{m}$ and P at the blowoff point); they may be compared with the value calculated from (3) using the experimental values of a and b:

$$(E/E_b)_{\max} = \frac{1 - 0.27/4}{1 + 0.70 - 0.27/2} = 0.59 \tag{5}$$

From Table 1 it can be seen that the actual value diverges from the calculated as mass flow and pressure are increased.

Table 1 Experimental values of $(E/E_b)_{\max}$ at arc blowoff

Orifice diam, in.	$\dot{m}$, lb/sec	P, psia	$(E/E_b)_{\max}$
0.375	0.23	290	0.57
	0.55	670	0.44
	0.77	830	0.39
1.0	1.0	160	0.50
	1.2	210	0.41
	1.3	240	0.35
	1.9	330	0.32
	3.4	600	0.29
1.5	7.3	470	0.30

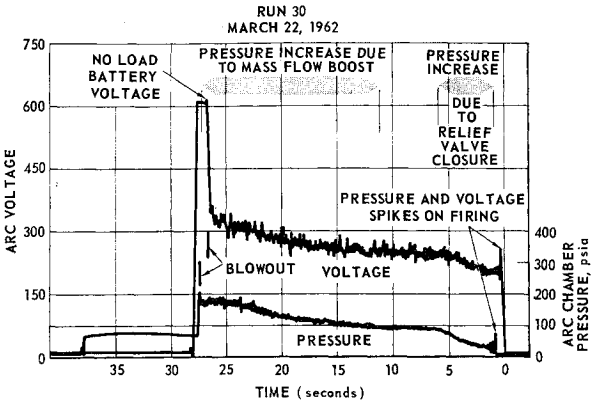

Fig. 5 Typical variable mass flow, pressure, and voltage traces showing starting transients.

The occurrence of observed low-frequency voltage swings of increasing magnitude, induced by the increasing aerodynamic disturbance of the arc, is felt to account for this fact. This is further supported by the evidence that the mean voltage appears to approach one-half the calculated maximum in the limit of large mass flow, as would be expected for a low-inductance circuit since the voltage cannot go very negative.

In Fig. 6 the predicted maximum pressure as a function of no-load battery potential is plotted as a straight line for the 1.0-in.-diam exit nozzle. The circles appearing on the graph are experimental blowoff points. The discrepancy results from the voltage swings as discussed in the previous paragraph. To achieve the data point corresponding to 660 psia chamber pressure, the unit was operated at 10.2-Mw power in the arc with 6.6 Mw into the gas at a weight flow of 3.3 lb-sec^{-1}.

As seen by the appearance of the fractional efficiency ϵ in Eq. (2), unless some knowledge of the transfer of heat to the emergent gas is available, the operation of the arc heater is not completely predictable. At present, a model based on radiation as the principal loss mechanism has successfully described the dependence of emergent gas enthalpy on mass flow and power in the region $P > 10$ atm. This dependence is indicated for the region $1.0 < \dot{m} < 5.0$ lb-sec^{-1} in Fig. 7.

Mach 7–10 Propulsion Tunnel

The size of the propulsion tunnel was broadly determined by the power available. A nozzle exit diameter of 15.16 in. was selected to provide a potential flow area near 1 ft^2. Of various nozzle designs, a simple sonic source has been favored by many, but the resulting streamwise Mach number variation $\partial M/\partial x$ in the working section was considered unsuitable for the expected model testing, so that a contoured nozzle with interchangeable throat sections was chosen. This "poly-Mach" concept had been used by Lee,[7, 8] who employed interchangeable throat sections followed by various polynomial contours in the design of nozzles for use with electrically heated air. The use of a conical entry nozzle followed by a transition section as discussed by Cresci[9] simplifies the machining of nozzles with small throats. Numerous profiles for different stagnation conditions for a range of Mach numbers between 7 and 10, using a program described by Conlan[10] for the computation of the potential flow nets, were therefore compared, and the feasibility of this approach for the desired tunnel stagnation conditions was demonstrated.

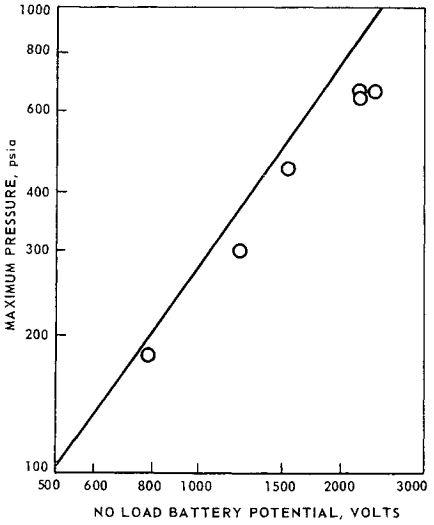

Fig. 7 Maximum pressure vs no-load battery potential.

The actual profile was based on Cresci's coordinates for the inviscid region, using a half-expansion angle of 8° at Mach 7, since agreement in contour shape is then reasonably close up to Mach 12. The best basis for boundary-layer estimation at hypersonic Mach numbers appeared to be the Lee correlation[7]

$$\frac{\delta^*}{l} = \frac{0.0064\, M^{1.25}}{(Re_l)^{0.14}} \qquad \text{with } \delta = 2.5\delta^*$$

which is similar to that given by Ruptash[11] for a two-dimensional nozzle in the region $1 < M < 7$. Here l is the contour length and M is the Mach number at exit from the nozzle. Since the second finite differences of slope showed too great a scatter, the profile was smoothed by substitution of a 10th order polynomial to obtain interpolated diameters at junctions in the hardware. The computed nozzle was also partly cut back to avoid unnecessary closure of the isentropic core. Separate throats were constructed for Mach 7 and 10 conditions, the design altitudes being 110,000 and 155,000 ft respectively (points close to the lower boundaries of the arc operating area shown in Fig. 1). These throats were made cylindrical, with $l^* = d^*$, in order to eliminate the usual Mach number disturbance that otherwise occurs on the axis of the working section.[7]

The liner of each throat section is made of beryllium copper; in order to preserve the supersonic contour, the liner is fixed to the stainless steel housing at the downstream-end and is free to expand toward the upstream-end by means of a sliding "O-ring" seal. The throat section is cooled by high-velocity, high-pressure water (blowdown system previously described in connection with electrode cooling). The Mach 7 throat has been operated at design conditions, but the operating capability of the Mach 10 throat is yet to be established.

With respect to heat transfer at the very high fluxes involved in the nozzle throats, some measurements have been

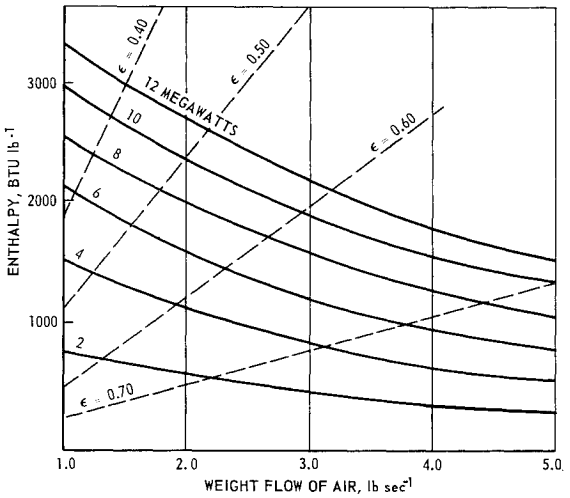

Fig. 6 Enthalpy vs weight flow at constant power.

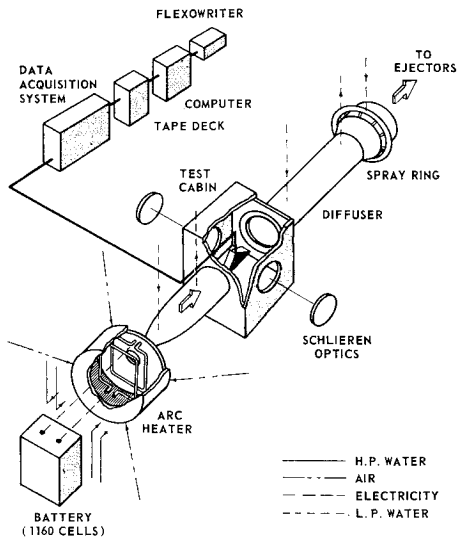

Fig. 8 Mach 7-10 arc-heated hypersonic propulsion tunnel.

obtained at fluxes up to 3.2 Btu-in.$^{-2}$-sec^{-1} in subsonic sections connected to arcs. Some of this work was done with straight tubes, and some with a convergent air-dilution and mixing section attached to an arc. In these cases, the data correlated well with the familiar Dittus and Boelter equation for fully developed turbulent pipe flow: $Nu = 0.023\ Re^{0.8}\ Pr^{0.33}$. One would not really expect this equation to apply for a nozzle throat, even one with a straight section, but if it were used to extrapolate to the Mach 10, 155 kft altitude conditions, it would predict a peak heat flux of approximately 45 Btu-in.$^{-2}$-sec^{-1} in the Mach 10 throat. Other estimates made by D. G. DeCoursin and F. W. Larsen of Fluidyne[¶] showed considerably higher heat fluxes (e.g., 90 Btu-in.$^{-2}$-sec^{-1} using the simplified Bartz[12] formula for nozzle heat transfer (reduced by the factor of $\frac{2}{3}$ to accord with experimental data for hot air) for the same Mach 10 conditions just considered).

Figure 8 schematically illustrates the remaining major components of the facility, which are largely conventional. The exit diffuser design relied largely on information provided by the investigation described by Harris and McCormick.[13] The diffuser has proved capable of better than normal shock recovery without a model in the test section (thereby permitting operation above the upper bound of Fig. 1), but the oscillation of the high-energy core has made it difficult to determine a representative average recovery figure.

An estimate of the variation of test section Mach number with simulated altitude has been made.** To do this, the variation of M with A/A^* over small ranges of M at $M = 7$ and 10 was first determined by computing a suitable range of profiles for each of several closely spaced Mach numbers at different altitudes, on the basis of flow continuity. After "smoothing" these results, a series of boundary layers at the various altitudes corresponding to values of M were "inserted" into the fixed geometry. Mach numbers for the various altitudes were then obtained from the A/A^* plot. Results obtained so far from running at Mach 7 appear to confirm the trend shown.

Figure 9, a typical Mach number traverse at a simulated altitude of 150,000 ft, shows a good agreement between the measured and the calculated boundary layer. To obtain such data, a water-cooled pitot probe was employed during

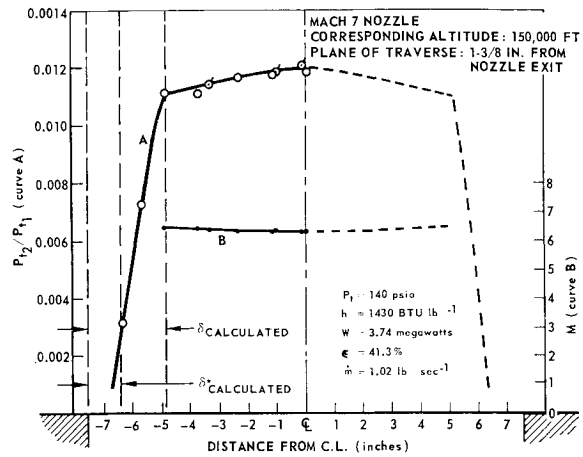

Fig. 9 Working section pressure traverse at 150,000 ft simulated altitude.

a run of approximately 2-min duration at constant stagnation pressure. Figure 10, which shows the relationship of simulated Reynolds numbers to the just described arc tunnel operating area and a possible flight corridor, clearly indicates the desirability of increasing the stagnation pressure to as high a value as possible in view of the closeness of the desired operating area to that for which the viscous interaction parameter $M^3/(Re)^{1/2}$ has a value greater than unity.[12] †† This aerodynamic consideration renders model testing increasingly undesirable at high Mach number if the Reynolds number is not simultaneously increased. It may be noted that the test rhombus will readily accommodate the characteristically slender form of hypersonic-cruise vehicle model suggested by the 1-ft streamwise dimension referred to in Fig. 10.

Summary

A form of d.c. arc unit embodying a single split-ring water-cooled electrode pair has been developed as a heater for a propulsion tunnel of approximately 1-ft^2 test section used in simulating the conditions of hypersonic flight in respect to

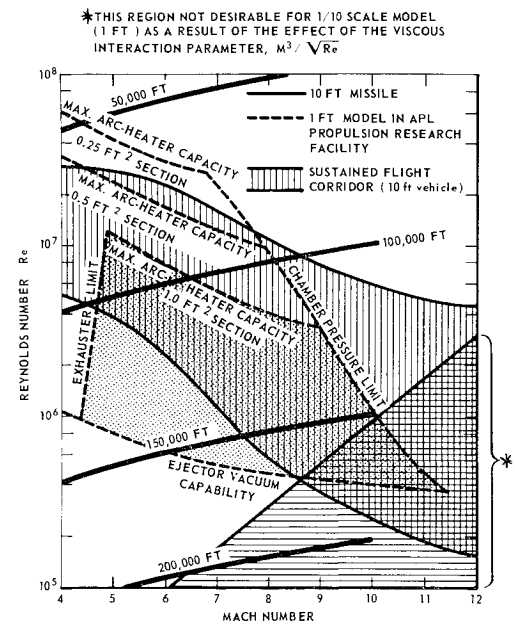

Fig. 10 Reynolds number simulation in APL Hypersonic Propulsion Laboratory. Use of a 10-ft scale for a model will drop the heater capacity outline by one cycle of *Re*.

¶ The detailed mechanical design and fabrication of the hypersonic tunnel were done by Fluidyne Engineering Corporation.

** Altitude data for altitudes above 155,000 ft were taken from Ref. 14.

†† Acknowledgment is made to R. Cramer for calling attention to this effect.

static pressure and temperature at altitudes between 90,000 and 220,000 ft. Operation has been demonstrated at pressures up to 1250 psia, running times up to 2 min, and input powers up to 10.2 Mw (at over 60% efficiency for the higher mass flows). Air weight flows up to 5.0 lb-sec^{-1} have been run. Units have also been employed for materials testing and in supersonic combustion experiments. The propulsion tunnel utilizes interchangeable throats to produce Mach 7 and 10 flows, the corresponding design altitudes being 110,000 and 155,000 ft. Good agreement between measured and calculated boundary layers has been demonstrated.

References

[1] Bunt, E. A., Bennett, L. W., Raezer, S. D., and Olsen, H. L., "Development of plasma arc heaters for hypersonic propulsion tunnels," Appl. Phys. Lab., The Johns Hopkins Univ., CM-984 (May 1961).

[2] Fehlner, L. F. and Nice, E. V., "Tabulation of standard atmospheres at 100-foot intervals of altitude," Appl. Phys. Lab., The Johns Hopkins Univ., TG-313-1 (August 1958).

[3] Feldman, S., "Hypersonic gas dynamic charts for equilibrium air," AVCO Everett Res. Lab. (January 1957).

[4] Reid, J. W., "High pressure arc jets," Am. Soc. Mech. Engrs. Paper 61-WA-246 (November 1961).

[5] Bonney, E. A., *Engineering Supersonic Aerodynamics* (McGraw-Hill Book Co., Inc., New York, 1950), p. 39.

[6] Hilsenrath, J., Klein, M., and Wooley, H. W., "Tables of thermodynamic properties of air to 15,000°K," Arnold Eng. Dev. Center TR-59-20 (December 1959).

[7] Lee, J. D., "Axisymmetric nozzles for hypersonic flow," Wright Air Dev. Center TN 59-228 (June 1959).

[8] Thomas, R. E. and Lee, J. D., "The Ohio State University 12-inch hypersonic wind tunnel system," Wright Air Dev. Center TN 59-228 (June 1959).

[9] Cresci, R. J., "Tabulation for coordinates for hypersonic axisymmetric nozzles," Wright Air Dev. Center TN 58-300, Part I (October 1958); Part II (July 1960).

[10] Conlan, J., "Real gas axisymmetric nozzle program operating instructions," Internal Memo., Naval Ordnance Lab., White Oak, Md. (October 31, 1960).

[11] Ruptash, J., "Growth of boundary layer in supersonic nozzles," *Symp. on High Speed Aerodynamics, Natl. Aeronaut. Establishment, Ottawa, Canada, February 1963* (University of Toronto, Canada, 1963), p. 42.

[12] Bartz, D. R., "A simple equation for rapid estimation of rocket nozzle convective heat transfer coefficients," Jet Propulsion **27**, 49 (1957).

[13] Harris, W. G. and McCormick, R. B., "Diffuser investigations in an axisymmetric open jet hypersonic wind tunnel," AGARD-Supersonic Tunnel Association Meeting, Marseilles, France (September 1959).

[14] Minzner, R. A. and Ripley, W. S., "The ARDC model atmosphere, 1956," Air Force Surveys in Geophys. no. 86, Air Force Cambridge Res. Center TN-56-204, Armed Services Tech. Inform. Agency Doc. 110233 (December 1956).

[15] Scheuing, R. A., Mead, H. R., Brook, J. W., Melnik, R. E., Hayes, W. D., Gray, K. E., Donaldson, C. DuP., Sullivan, R. D., "Theoretical prediction of pressures in hypersonic flow with special reference to configurations having attached leading-edge shock, part I, theoretical investigation," Aeronaut. Systems Div. TR 61-60 (May 1962).

MARCH-APRIL 1964 J. SPACECRAFT VOL. 1, NO. 2

Gridding of Satellite Observations

R. G. DeBiase*
General Electric Company, Philadelphia, Pa.

Gridding is the association of earth coordinates with satellite observations. This paper describes a geometrical method for gridding the pictorial frames of cloud data obtained by the vidicon system in the Nimbus Satellite. It is shown that the particular formulation of the problem leads to an explicit bilateral mapping procedure between earth coordinates and image plane coordinates that has desirable computational consequences. Results of a typical gridding computation are presented.

Nomenclature

X, Y, Z	= coordinates of geocentric inertial axis system
D	= distance from origin of geocentric inertial axis system to satellite
R, P, W	= local coordinate system on the satellite orbit, with R and W axes in orbit plane
X', Y', Z'	= body axes; origin is coincident with origin of the R, P, W axes
$\bar{X}, \bar{Y}$	= normalized variables that range between -1 and $+1$, in traversing the camera image planes
e	= subscripted, denotes unit vector along specified coordinate axis
$P\bar{X}, P\bar{Y}$	= scanning planes that sweep the cameras, specified by a line of constant $\bar{X}$ or $\bar{Y}$ and a point at center of camera lens
$U\bar{X}, U\bar{Y}$	= unit normals to the $P\bar{X}, P\bar{Y}$ planes, respectively
ϕ, θ	= surface coordinates (latitude and longitude, respectively) on nonrotating earth model
ϕ', θ'	= latitude and longitude, respectively, on rotating earth model
λ, μ, ν	= direction cosines relative to inertial axes
λ', μ', ν'	= direction cosines relative to body axes
Ω	= longitude of ascending node, deg
i	= angle of inclination, deg
$\theta_R, \theta_P, \theta_W$	= angles of roll, pitch, and yaw
ω_e	= earth's angular velocity

Received June 7, 1963; revision received January 10, 1964. Developed under NASA Contract NAS5-3116. The author is indebted to L. Byrne of the NASA Goddard Space Flight Center for his encouragement and support of the method. H. Jung of General Electric provided the competent programming assistance to reduce the ideas to an efficient computational scheme.

* Applied Mathematician, Space Technology Center; now Member, Technical Staff, Aerospace Corporation, Los Angeles, Calif.

Introduction

A MAJOR problem inherent in the use of satellites for observation purposes is the difficulty of "gridding" an observed event, i.e., relating it to a geographic point on the earth. To know that a cyclonic formation exists is certainly of less value than knowing that a cyclonic formation is present in the Texas panhandle. Pinpointing observations geographically also affords a dynamic interpretation